End Point of Black Ring Instabilities and the Weak Cosmic Censorship Conjecture

Pau Figueras,[1,*] Markus Kunesch,[2,†] and Saran Tunyasuvunakool[2,‡]
[1]School of Mathematical Sciences, Queen Mary University of London, Mile End Road, London E1 4NS, United Kingdom
[2]Department of Applied Mathematics and Theoretical Physics (DAMTP), Centre for Mathematical Sciences, University of Cambridge, Wilberforce Road, Cambridge CB3 0WA, United Kingdom

(Received 24 December 2015; published 18 February 2016)

We produce the first concrete evidence that violation of the weak cosmic censorship conjecture can occur in asymptotically flat spaces of five dimensions by numerically evolving perturbed black rings. For certain thin rings, we identify a new, elastic-type instability dominating the evolution, causing the system to settle to a spherical black hole. However, for sufficiently thin rings the Gregory-Laflamme mode is dominant, and the instability unfolds similarly to that of black strings, where the horizon develops a structure of bulges connected by necks which become ever thinner over time.

DOI: 10.1103/PhysRevLett.116.071102

Introduction.—Black holes are amongst the most important solutions of the Einstein equations. Despite their simplicity, they capture some of the most fundamental aspects of the theory. The black holes of general relativity also play a key role in astrophysics, in particular as a description of the compact dark objects at the center of galaxies. This relies on the assumption that they are nonlinearly stable to small perturbations. Although the full nonlinear stability of the Kerr solution [1] has not been rigorously proven, there is good evidence that it is indeed stable [2–5].

The situation is markedly different in higher dimensions, where black holes can be dynamically unstable to gravitational perturbations. This was first shown by Gregory and Laflamme [6] in the case of black strings and black p-branes. Their result was later generalized to boosted black strings [7]. In a remarkable paper [8], Lehner and Pretorius used numerical relativity techniques to study the nonlinear evolution of the Gregory-Laflamme (GL) instability of the five-dimensional black string. They found that the instability unfolds in a self-similar process which gives rise to a sequence of black hole "bulges" connected by black strings which become ever thinner over time. Furthermore, they provided convincing evidence that this process would lead to these thin strings completely pinching off within finite time. This result was interpreted as evidence for a violation of the weak cosmic censorship conjecture (WCC) [9,10] in spacetimes with compact extra dimensions.

Another novel aspect of higher dimensional black hole physics is that horizons can have nonspherical topologies, even in asymptotically flat spaces. The five-dimensional black ring of Emparan and Reall [11,12] is the first example. This is a stationary solution of the vacuum Einstein equations with horizon topology $S^1 \times S^2$. The S^1 of the ring is a contractible circle that is stabilized by the centrifugal force provided by the rotation. In terms of the standard dimensionless "thickness" parameter ν [12], black rings can be classified as either "thin" $(0 < \nu < 0.5)$ or "fat" $(0.5 < \nu < 1)$. This thickness parameter describes the relative sizes between the S^1 and the S^2 of the ring. Fat rings are known to be unstable under radial perturbations [13,14]. Very recently, thin rings have been shown to be linearly subject to a GL-like instability [15,16]. Given the similarities between very thin black rings and boosted black strings, it is plausible that the nonlinear evolution of the GL instability on thin rings would proceed in a similar manner to that on black strings, thus leading to a violation of WCC in asymptotically flat spaces. This possibility has been contemplated in the past [13,15,16]. Arguably, the resolution of WCC is one of the greatest open problems in classical general relativity, as it directly affects the predictability of the theory.

In this Letter, we report on the end state of black ring instabilities through fully nonlinear, numerical evolution. For very fat rings, the dominant instability is the axisymmetric ("radial") mode found in Ref. [14]. Rings with $0.2 \lesssim \nu \lesssim 0.6$ are unstable under a new type of nonaxisymmetric instability which deforms the shape of the ring without substantially changing its thickness. In analogy with blackfolds [17], we call it an *elastic* mode. In these two regimes, the end point of the instability is the topologically spherical Myers-Perry (MP) black hole. On the other hand, for very thin rings $(\nu \lesssim 0.15)$ the GL instability dominates. Our main focus here will be on thin rings, where our results suggest that the WCC does not hold in the neighborhood of sufficiently thin rings. A more detailed discussion of our results for fatter rings, and a comparison of different angular perturbation modes, will be presented elsewhere [18].

Numerical approach.—We use the CCZ4 formulation of the five-dimensional Einstein vacuum equations [19,20] in Cartesian coordinates (x, y, z, w), with the redefinition of the damping parameter $\kappa_1 \to \kappa_1/\alpha$, where α is the lapse [21]. We choose $\kappa_1 = 0.1$ and $\kappa_2 = 0$. We have

experimented with other values, but the results do not change. We evolve perturbations of singly spinning black rings which only break the $U(1)$ symmetry in the $x-y$ rotational plane. The remaining $U(1)$ symmetry in the orthogonal $z-w$ plane is exploited to dimensionally reduce the CCZ4 equations to $(3+1)$-dimensions using the modified cartoon method [22,23]. We do not expect that breaking this orthogonal $U(1)$ symmetry will be relevant in the context of this work.

As initial data, we start with the stationary ring of Ref. [11] in the isotropic coordinates introduced in Ref. [14]. This allows us to transform this solution into Cartesian coordinates. We introduce a small amount of $m=2$ (in the nomenclature of Ref. [15]) nonaxisymmetric perturbation in the conformal factor χ via

$$\chi = \chi_0 \left[1 + A \frac{1}{(1+Y^2)^{\frac{3}{2}}} \frac{x^2-y^2}{\Sigma} \right], \tag{1}$$

where χ_0 is the unperturbed conformal factor of the stationary black ring, A is the perturbation amplitude, and

$$\Sigma = \sqrt{(\tilde{R}^2+r^2)^2 - 4\tilde{R}^2(x^2+y^2)}, \qquad r = \sqrt{x^2+y^2+z^2}$$
$$Y = \frac{4(1-\nu)\Sigma}{\nu(r^2+\tilde{R}^2-\Sigma)}, \qquad \tilde{R} = R\sqrt{(1-\nu)/(1+\nu^2)}. \tag{2}$$

Here $0<\nu<1$ and $R>0$ are the ring's thickness and radius parameters, respectively. In our simulations, we fix $\tilde{R}=1$ and vary ν. This ensures that the initial coordinate radius of the black ring is roughly 1 for all values of ν, but the mass and hence the instability time scale will vary.

Our initial condition violates the Hamiltonian and momentum constraint equations. However, by using small values of A, we can ensure that constraint violations in the initial data are correspondingly small. These small constraint violations are quickly suppressed by the damping terms in the CCZ4 equations. In our simulations, we choose $10^{-6} \leq A \leq 0.002$. The radial dependence of the perturbation (1) is chosen to ensure that it is localized on the horizon and therefore does not change the mass nor the angular momentum of the background spacetime.

In our coordinates, $\Sigma=0$ is a coordinate singularity that corresponds to another asymptotically flat region at the other side of the Einstein-Rosen bridge. We regulate this singularity using the "turduckening" approach [24,25] by manually restricting to $\Sigma \geq \epsilon^2$, for some small ϵ. We choose ϵ such that the width of the region in which Σ is modified is at most 50% of the unperturbed ring's horizon.

To evolve the lapse, we use the CCZ4 $(1+\log)$ slicing [19] with an advection term, starting from the initial condition $\alpha=\chi$. However, we could not use the standard Gamma-Driver shift condition [26] as it quickly freezes the large initial values of $\tilde{\Gamma}^i$, even with advection terms. Instead, we evolve the shift using

$$\partial_t \beta^i = F(\tilde{\Gamma}^i - f(t)\tilde{\Gamma}^i_{t=0}) - \eta(\beta^i - \beta^i_{t=0}) + \beta^k \partial_k \beta^i, \tag{3}$$

where $\tilde{\Gamma}^i$ is the evolved conformal connection function and

$$f(t) = \exp\left[-(\delta_1 Y^2 + \delta_2)t^2/M\right], \tag{4}$$

Y is as defined in Eq. (2), δ_1 and δ_2 are dimensionless parameters, and M is the mass of the unperturbed ring. For our simulations we use $F=2/3$, $\eta=1$, $\delta_1=0.25$, and $\delta_2=0.1$. The initial shift is taken to be χ times the analytic shift.

We evolve the CCZ4 equations numerically on an adaptively refined mesh using the GRChombo code [27,28]. We discretize the equations in space using fourth order finite differences and integrate in time with RK4. We use between 8 to 13 levels of refinement depending on the thickness of the ring. The finest resolution is chosen such that the interior of the horizon is never covered by less than 50 grid points after gauge adjustment. At the outer boundaries we impose periodic boundary conditions. However, the spatial extent of the domain is made sufficiently large so as to avoid spurious boundary effects throughout the course of the simulation.

To stop the formation of large gradients in $\tilde{\gamma}_{ij}$ close to the ring singularity, we add a new diffusion term to the CCZ4 equations, which is restricted to act only inside a region amounting to less than 50% of the horizon's interior. This is reminiscent of *shock-capturing* techniques in computational fluid dynamics [29]. The additional term does not change the evolution outside the horizon since we have enough grid points across the horizon and the diffusion term only affects features at very small scales. See the Supplemental Material [30] for more details.

Results.—For rings with $0.3 \lesssim \nu \lesssim 0.6$, we find that the evolution is dominated by a new nonaxisymmetric mode which is distinct from the GL mode identified in Ref. [15]. Note that this range includes both thin and fat rings. In the nonlinear regime, this new mode deforms the ring without substantially changing its thickness. We identify it as an elastic mode. In Fig. 2(a) we display a snapshot of the apparent horizon for a ring with $\nu=0.4$ in the highly nonlinear regime of the evolution. The deformation caused by the elastic mode can also be seen in Fig. 2 (top left). The divergence between the maximum and minimum S^1 radii shows that the ring is physically stretching. To measure the influence of the GL mode, we look at the degree of nonuniformity *along* the ring by plotting the maximum and minimum radius of the S^2 of the ring as measured by cross-sectional area. The result is shown in Fig. 2 (top right). For rings in this range of ν, the minimum S^2 radius never decreases substantially, and the growth rate of the elastic mode is larger than the GL mode. The latter is therefore completely irrelevant as far as the nonlinear dynamics is concerned. In fact, the growth rate of the GL mode decreases as the rings become fatter, and for

$0.4 \lesssim \nu \lesssim 0.6$ the complete gravitational waveforms show that only the elastic mode is relevant. This new instability always ends in a collapse into a topologically spherical MP black hole.

For thin rings with $0.2 \lesssim \nu \lesssim 0.35$, we observe a competition between different modes. The waveform in Fig. 1 (top) shows that, in the linear regime, there is an apparent mode mixing until nonlinearities become important. To gain a better understanding of the various modes in the $m = 2$ sector of nonaxisymmetric gravitational perturbations, we extract the waveforms by monitoring

$$h_+ = \frac{\tilde{\gamma}_{xx} - \tilde{\gamma}_{yy}}{2} \left(\frac{r}{\tilde{R}}\right)^{(3/2)}, \tag{5}$$

along the z axis. From this, we can identify the frequencies and growth rates of the two modes by fitting the data to

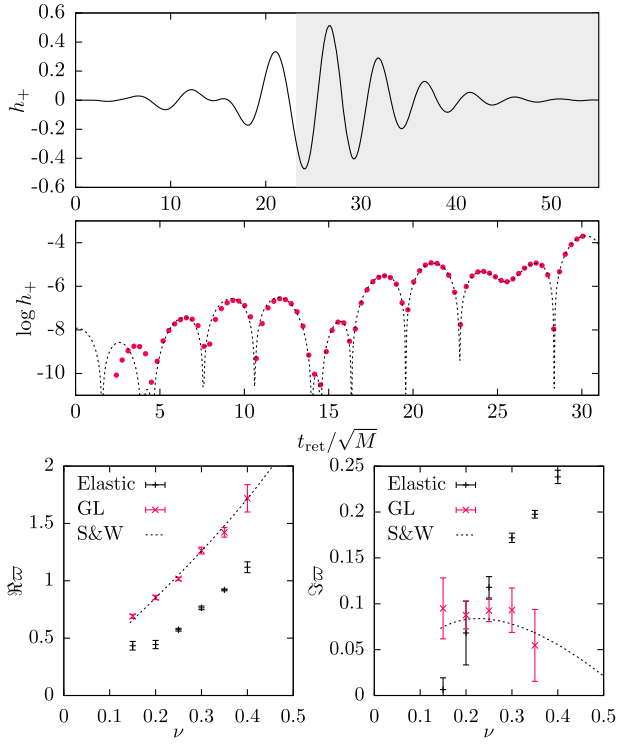

FIG. 1. Top: complete gravitational waveform for the evolution of the $\nu = 0.25$ ring perturbed with an $m = 2$ mode with amplitude $A = 5 \times 10^{-4}$. The shaded part corresponds to the portion of the evolution where the outermost apparent horizon has spherical topology. Middle: fit (6) of the actual data in the linear regime (red dots) for a perturbation with amplitude $A = 10^{-5}$. At the early stages of the evolution there is contamination from constraint violating modes. Bottom: Real (left) and imaginary (right) parts of the frequency $\varpi \equiv \omega/(2\pi T)$ of the gravitational waves in the linear regime. Here, T is the temperature of the unperturbed ring. The dashed lines correspond to the results of Ref. [15]. For $\nu = 0.4$ we could not reliably extract the growth rate of the GL mode.

$$A_1 \sin(\Re\varpi_1 t + \varphi_1) e^{\Im\varpi_1 t} + A_2 \sin(\Re\varpi_2 t + \varphi_2) e^{\Im\varpi_2 t}. \tag{6}$$

We give further details about our fitting procedure and error estimation in the Supplemental Material [30]. In Fig. 1 (middle) we compare the data with the fit (6) to show that they are in very good agreement. This confirms that the linear dynamics is governed by the two modes that we have identified. In Fig. 1 (bottom) we display the frequencies and growth rates of both the elastic and GL $m = 2$ modes. Our results for the GL mode agree very well with Ref. [15]; however, we were only able to identify the GL mode for thin enough rings ($\nu \lesssim 0.4$). For thicker rings, the growth rate of the GL mode is much slower than that of the elastic mode, and hence it is much harder to isolate in a fully nonlinear evolution. The fitting procedure also allows us to estimate the amplitude of each mode in our initial data (1). Both $m = 2$ modes have comparable amplitudes initially, and therefore, our simulation is not biased towards the newly identified elastic mode.

Since both modes have similar growth rates for $0.2 \lesssim \nu \lesssim 0.35$, it is not surprising that the nonlinear dynamics is governed by a combination of the two. Figure 2 (top left) shows a significant divergence in S^1 radii for a $\nu = 0.2$ ring on a much larger scale than the ring's thickness. This is indicative of the elastic mode

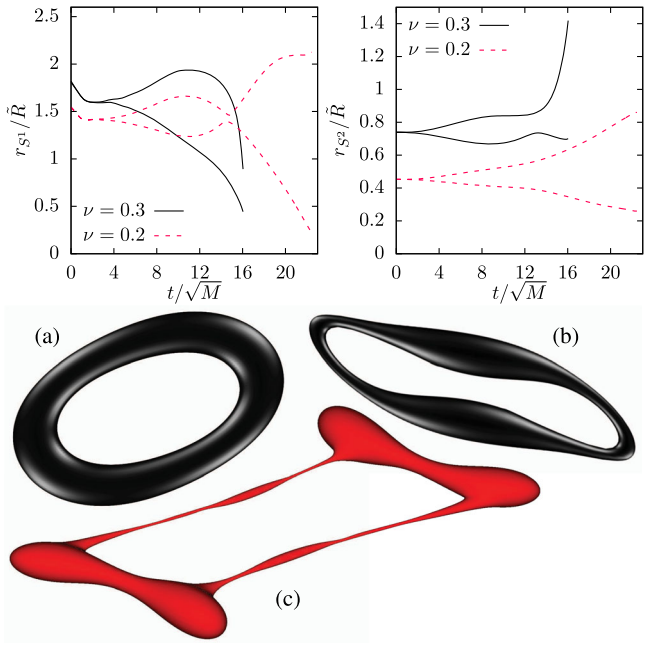

FIG. 2. Top left: maximum and minimum inner radius of the S^1 of the ring, as measured by the geodesic distance from the center of the ring to the apparent horizon. For $\nu = 0.2$ the maximum and the minimum eventually switch due to the displacement of the bulges. Top right: maximum and minimum areal radius of the S^2 of the ring. (a) Apparent horizon of a $\nu = 0.4$ ring in the highly dynamical stages of the evolution. (b) Apparent horizon of the $\nu = 0.2$ ring just before the collapse into a spherical black hole. (c) $\chi = 0.2$ contour for a $\nu = 0.15$ ring during the evolution.

dynamics. On the other hand, in Fig. 2 (top right) we observe that GL dynamics causes this ring to also become highly nonuniform. The combined effect of these two modes on the apparent horizon is shown in Fig. 2(b). Even though the GL mode does grow significantly here, the end point is still a MP black hole. Presumably, the deformations due to the elastic mode enhance the efficiency of the gravitational wave emission, allowing the ring to quickly shed angular momentum and mass and collapse into a spherical black hole. Therefore, no violation of WCC is observed in this particular case.

For rings with $\nu \lesssim 0.15$, the GL mode grows fastest and thus dominates the dynamics. In this regime, we consider the nonlinear evolution of a $\nu = 0.15$ ring with an $m = 2$ perturbation with amplitude $A = 5 \times 10^{-5}$. It turns out that for such thin rings, the $m = 4$ mode grows fast enough that excitations from numerical noise also become important. Therefore, we find that the *generic* nonlinear dynamics is governed by a combination of these two modes. In the highly nonlinear regime the apparent horizon consists of big bulges connected by long and thin necks. One would expect that the thin necks should themselves eventually become GL unstable, giving rise to a second generation of bulges connected by even thinner necks. For such highly deformed dynamical rings, the apparent horizon is no longer a single-valued function $Y: S^1 \times S^2 \to \mathbb{R}$, causing our horizon finder to fail (see Supplemental Material [30]). However, in our gauge the apparent horizon follows certain contours of the conformal factor, χ. We use these as an indication of the location and shape of the apparent horizon in lieu of the actual surface. In Fig. 2(c) we display the $\chi = 0.2$ contour for the $\nu = 0.15$ ring for an $m = 2$ perturbation with $A = 5 \times 10^{-5}$ at $t/\sqrt{M} = 33.87$. This shows clear evidence that a new generation of bulges has formed along the thin necks. We could not continue the evolution due to the limitation in our computational resources, but our results provide enough evidence that this instability should continue in a qualitatively similar manner as in the static black string. More precisely, the horizon should develop a fractal structure consisting of big bulges connected by thin necks at different scales. The thinnest necks should reach zero size, and hence a naked singularity should form, in finite asymptotic time. Since there is no fine-tuning involved, this result provides evidence that WCC is violated near thin enough black ring spacetimes. We note that a pure $m = 4$ perturbation also gives rise to a similar structure. However, without the stretching effect from $m = 2$ the instability's time scale is much longer as the necks are shorter. Significant additional resources will be required to reach the second generation of bulges in this case; however, there is no reason to expect that the end point should be any different. The $m = 1$ and higher m modes are also unstable and their study will be presented elsewhere [18].

Conclusions.—We have studied the nonlinear dynamics of thin and fat black rings under nonaxisymmetric perturbations. For rings with $\nu \gtrsim 0.2$ the end point of the instabilities is a MP black hole with a lower angular momentum than the original ring. On the other hand, the GL instability dominates the evolution of thin enough ($\nu \lesssim 0.15$) rings, and the end point should be the pinch-off of the ring. This indicates that WCC is violated around these black ring spacetimes. Note that for these rings the dimensionless angular momentum [12] is not particularly large, $j \sim 1.12$. Therefore, our results suggest that violations of WCC can occur for asymptotically flat black holes with j of order 1. Even though we have only considered the $D = 5$ case, this conclusion should extend to higher dimensions.

We have also identified a new, elastic-type of instability in five-dimensional black rings. This had not been anticipated and was not seen in Refs. [15,16]. However, it plays a crucial role in the end point of generic nonaxisymmetric instabilities as it dominates for rings with $\nu \gtrsim 0.2$. It would be very interesting to do a more thorough analysis of the nonaxisymmetric gravitational perturbations of black rings and get a detailed understanding of these elastic instabilities.

Finally, we introduced a robust and simple new method, based on localized diffusion, to handle singularities in numerical general relativity. While it is used in conjunction with the moving puncture method in the present work, we anticipate that it has a wider range of applications. We will present a more detailed analysis of this in future work [42].

We are very grateful to Garth Wells (Dept. Engineering, U. Cambridge) for suggesting to us the shock capturing technique which has proven so valuable in this work. We would like to thank J. Briggs, J. Camps, R. Emparan, J. Jäykkä, K. Kornet, L. Lehner, F. Pretorius, H. Reall, E. Schnetter, U. Sperhake, T.Wiseman, and H. Witek for numerous stimulating discussions. P. F. would like to especially thank E. Schnetter and U. Sperhake for early collaboration in this project. We are very grateful to our collaborators and co-developers of the GRChombo code, K. Clough, E. Lim, and H. Finkel. We would also like to thank J. Santos and B. Way for allowing us to display their data in Fig. 1. A significant part of this work was undertaken on the COSMOS Shared Memory system at DAMTP, University of Cambridge, operated on behalf of the STFC DiRAC HPC Facility. This equipment is funded by BIS National E-infrastructure capital Grant No. ST/J005673/1 and STFC Grants No. ST/H008586/1, No. ST/K00333X/1. Further portions of this research were conducted with high performance computational resources provided by Louisiana State University [31] on its SuperMike-II cluster under allocation NUMREL06. The authors also acknowledge HPC resources from the NSF-XSEDE Grant No. PHY-090003, provided by the Texas Advanced Computing Center (TACC) at The University of

Texas at Austin on its Stampede cluster, and by the San Diego Supercomputer Center (SDSC) at UC San Diego on its Comet cluster. P. F. and S. T. were supported by the European Research Council Grant No. ERC-2011-StG 279363-HiDGR. P. F. was also supported by the Stephen Hawking Advanced Research Fellowship from the Centre for Theoretical Cosmology, University of Cambridge. P. F. is currently supported by a Royal Society University Research Fellowship and by the European Research Council Grant No. ERC-2014-StG 639022-NewNGR. M. K. is supported by an STFC studentship. P. F. wants to thank Perimeter Institute and Princeton University for hospitality during various stages of this work.

*Also at DAMTP, Centre for Mathematical Sciences, Wilberforce Road, Cambridge CB3 0WA, United Kingdom.p.figueras@qmul.ac.uk
†m.kunesch@damtp.cam.ac.uk
‡s.tunyasuvunakool@damtp.cam.ac.uk

[1] R. P. Kerr, Phys. Rev. Lett. **11**, 237 (1963).
[2] B. F. Whiting, J. Math. Phys. (N.Y.) **30**, 1301 (1989).
[3] M. Dafermos and I. Rodnianski, arXiv:1010.5132.
[4] M. Dafermos, I. Rodnianski, and Y. Shlapentokh-Rothman, arXiv:1402.7034.
[5] M. Dafermos, I. Rodnianski, and Y. Shlapentokh-Rothman, arXiv:1412.8379.
[6] R. Gregory and R. Laflamme, Phys. Rev. Lett. **70**, 2837 (1993).
[7] J. L. Hovdebo and R. C. Myers, Phys. Rev. D **73**, 084013 (2006).
[8] L. Lehner and F. Pretorius, Phys. Rev. Lett. **105**, 101102 (2010).
[9] R. Penrose, Riv. Nuovo Cimento **1**, 252 (1969) [Gen. Relativ. Gravit. **34**, 1141 (2002)].
[10] D. Christodoulou, Classical and Quantum Gravity **16**, A23 (1999).
[11] R. Emparan and H. S. Reall, Phys. Rev. Lett. **88**, 101101 (2002).
[12] R. Emparan and H. S. Reall, Classical and Quantum Gravity **23**, R169 (2006).
[13] H. Elvang, R. Emparan, and A. Virmani, J. High Energy Phys. 12 (2006) 074.
[14] P. Figueras, K. Murata, and H. S. Reall, Classical and Quantum Gravity **28**, 225030 (2011).
[15] J. E. Santos and B. Way, Phys. Rev. Lett. **114**, 221101 (2015).
[16] K. Tanabe, arXiv:1510.02200.
[17] R. Emparan, T. Harmark, V. Niarchos, and N. A. Obers, J. High Energy Phys. 03 (2010) 063.
[18] P. Figueras, M. Kunesch, and S. Tunyasuvunakool (to be published).
[19] D. Alic, C. Bona-Casas, C. Bona, L. Rezzolla, and C. Palenzuela, Phys. Rev. D **85**, 064040 (2012).
[20] A. Weyhausen, S. Bernuzzi, and D. Hilditch, Phys. Rev. D **85**, 024038 (2012).
[21] D. Alic, W. Kastaun, and L. Rezzolla, Phys. Rev. D **88**, 064049 (2013).
[22] F. Pretorius, Classical and Quantum Gravity **22**, 425 (2005).
[23] M. Shibata and H. Yoshino, Phys. Rev. D **81**, 104035 (2010).
[24] D. Brown, O. Sarbach, E. Schnetter, M. Tiglio, P. Diener, I. Hawke, and D. Pollney, Phys. Rev. D **76**, 081503 (2007).
[25] D. Brown, P. Diener, O. Sarbach, E. Schnetter, and M. Tiglio, Phys. Rev. D **79**, 044023 (2009).
[26] M. Alcubierre, B. Brügmann, P. Diener, M. Koppitz, D. Pollney, E. Seidel, and R. Takahashi, Phys. Rev. D **67**, 084023 (2003).
[27] K. Clough, P. Figueras, H. Finkel, M. Kunesch, E. A. Lim, and S. Tunyasuvunakool, Classical and Quantum Gravity **32**, 245011 (2015).
[28] M. Adams, P. Colella, D. Graves, J. Johnson, N. Keen, T. Ligocki, D. Martin, P. McCorquodale, D. Modiano, P. Schwartz, T. Sternberg, and B. Van Straalen, Lawrence Berkeley National Laboratory Technical Report No. LBNL-6616E, 2015 (unpublished).
[29] A. Lapidus, J. Comput. Phys. **2**, 154 (1967).
[30] See Supplemental Material at http://link.aps.org/supplemental/10.1103/PhysRevLett.116.071102 for numerical checks and further technical details, which includes Refs. [32–42].
[31] http://www.hpc.lsu.edu
[32] U. Sperhake, E. Berti, V. Cardoso, and F. Pretorius, Phys. Rev. Lett. **111**, 041101 (2013).
[33] M. Zilhao, H. Witek, U. Sperhake, V. Cardoso, L. Gualtieri, C. Herdeiro, and A. Nerozzi, Phys. Rev. D **81**, 084052 (2010).
[34] H. Witek, Ph.D. thesis, IST/CENTRA Lisbon, 2012; arXiv:1307.1145.
[35] J. Donea and A. Huerta, *Finite Element Methods for Flow Problems* (John Wiley & Sons, New York, 2003).
[36] J. Von Neumann and R. D. Richtmyer, J. Appl. Phys. **21**, 232 (1950).
[37] J. Thornburg, Living Rev. Relativity **10** (2007).
[38] S. Balay, W. D. Gropp, L. C. McInnes, and B. F. Smith, in *Modern Software Tools in Scientific Computing*, edited by E. Arge, A. M. Bruaset, and H. P. Langtangen (Birkhäuser, Springer, New York, 1997), p. 163.
[39] S. Balay, S. Abhyankar, M. F. Adams, J. Brown, P. Brune, K. Buschelman, L. Dalcin, V. Eijkhout, W. D. Gropp, D. Kaushik, M. G. Knepley, L. C. McInnes, K. Rupp, B. F. Smith, S. Zampini, and H. Zhang, Argonne National Laboratory Technical Report No. ANL-95/11—Revision 3.6, 2015 (unpublished).
[40] E. H. W. Meijering, K. J. Zuiderveld, and M. A. Viergever, IEEE Trans. Image Process. **8**, 192 (1999).
[41] O. J. C. Dias, G. S. Hartnett, and J. E. Santos, Classical and Quantum Gravity **31**, 245011 (2014).
[42] P. Figueras, M. Kunesch, S. Tunyasuvunakool, and G. Wells (to be published).